Lifetime of muscarinic receptor–G-protein complexes determines coupling efficiency and G-protein subtype selectivity

Olga S. Ilyaskina[a], Horst Lemoine[b], and Moritz Bünemann[a,1]

[a]Department of Pharmacology and Clinical Pharmacy, Faculty of Pharmacy, University of Marburg, 35032 Marburg, Germany; and [b]Department of Laser Medicine, Heinrich Heine University, 40225 Düsseldorf, Germany

Edited by Brian K. Kobilka, Stanford University School of Medicine, Stanford, CA, and approved March 30, 2018 (received for review September 7, 2017)

G-protein–coupled receptors (GPCRs) are essential for the detection of extracellular stimuli by cells and transfer the encoded information via the activation of functionally distinct subsets of heterotrimeric G proteins into intracellular signals. Despite enormous achievements toward understanding GPCR structures, major aspects of the GPCR–G-protein selectivity mechanism remain unresolved. As this can be attributed to the lack of suitable and broadly applicable assays, we set out to develop a quantitative FRET-based assay to study kinetics and affinities of G protein binding to activated GPCRs in membranes of permeabilized cells in the absence of nucleotides. We measured the association and dissociation kinetics of agonist-induced binding of $G_{i/o}$, $G_{q/11}$, G_s, and $G_{12/13}$ proteins to muscarinic M_1, M_2, and M_3 receptors in the absence of nucleotides between fluorescently labeled G proteins and receptors expressed in mammalian cells. Our results show a strong quantitative correlation between not the on-rates of G-protein–M_3–R interactions but rather the affinities of G_q and G_o proteins to M_3–Rs, their GPCR–G-protein lifetime and their coupling efficiencies determined in intact cells, suggesting that the G-protein subtype-specific affinity to the activated receptor in the absence of nucleotides is, in fact, a major determinant of the coupling efficiency. Our broadly applicable FRET-based assay represents a fast and reliable method to quantify the intrinsic affinity and relative coupling selectivity of GPCRs toward all G-protein subtypes.

GPCR | G-protein selectivity | G-protein affinity | FRET | muscarinic

G-protein–coupled receptors (GPCRs) are involved in many physiological functions and represent the largest receptor family, accounting for more than several hundred members. These receptors couple to four major G-protein classes (G_i, $G_{q/11}$, G_s, and $G_{12/13}$) (1), which are defined by the type of Gα subunit. In total, we have a pool of 16 α, 5 β, and 12 γ subunits (2). At the same time, active G proteins are able to interact with more than 25 different effectors, such as adenylyl cyclases, ion channels (3), PLC, RhoGEFs (4, 5), and PDE (4), further enhancing the complexity of GPCR signaling. Although many classes of G proteins exhibit a high degree of selectivity by the given GPCR, it has been shown that the same receptor can couple to more than one class of G proteins (6–11). Such a large number of potential combinations gives rise to the question of how the receptor actually finds the right G protein.

Breakthroughs in GPCR crystallization gave detailed insight into the GPCR structures (12, 13) and GPCRs' activation and interaction with downstream partners. However, the selectivity of receptor–G-protein coupling and its underlying mechanisms remain unclear (14, 15). In our study, we decided to focus on muscarinic receptors (mAChRs), which belong to class A GPCRs and constitute a family with five subtypes (16). M_1– and M_3–Rs are classic G_q coupling GPCRs (17–20); however, changes in the concentration of second messengers after treatment with pertussis and cholera toxins (17, 21–25) suggest a possible coupling to G_i and G_s proteins. In contrast, M_2–R is a classic G_i family-coupled receptor (19, 23, 26). Despite the fact that mAChRs couple to different G-protein classes, the comparison of crystal structures of these GPCRs revealed only small differences in transmembrane helices (12, 13, 27), meaning that the current knowledge of receptor structures restricts a prediction of the coupling to a particular G-protein class or subtype (28, 29).

In accordance with ternary complex model agonist, receptor and G protein remain stably coupled until GTP binds to the Gα subunit and immediately triggers G-protein activation and its dissociation from the receptor (30, 31). We hypothesized that the mechanism underlying the coupling selectivity must be encoded in the receptor–G-protein interaction. Therefore, we set out to measure the kinetics and affinity of the GPCR–G-protein interaction in the absence of nucleotides to determine the affinity of the G proteins to the receptors in a quantitative manner. Due to the high concentration of nucleotides in the cytosol, the ternary complex has a very short lifetime (32); therefore, previous methods to measure the GPCR–G-protein affinity were mostly based on biochemical assays and required complicated protein purification steps (8, 33–35). In this study, we establish a reliable FRET-based method for quantification of the G-protein affinity to the receptor in a regular plasma membrane environment. With this method, we measured on- and off-rates as well as steady-state binding curves for the agonist-driven interaction of GPCRs with representative G proteins from all four classes.

Results

Studying Ternary Complex Formation by Means of FRET. To investigate the affinity of receptor–G-protein interaction, the dynamics of G proteins binding to activated GPCRs and their subsequent

Significance

The family of G-protein–coupled receptors (GPCRs) is the largest receptor family, and each member detects specific ligands, which in turn, activate selected members of one or more G-protein families. We developed a broadly applicable assay to study the specificity of GPCR–G-protein interaction in a subtype selective manner. We were able to quantitatively measure both association and dissociation rates of G proteins from agonist-activated GPCRs. We found that the stability of the receptor–G-protein complex is an inherent property of both interaction partners independent on the agonist used. Furthermore, its lifetime correlated closely with the ability of the receptor to activate the corresponding G-protein subtype.

Author contributions: O.S.I., H.L., and M.B. designed research; O.S.I. performed research; H.L. and M.B. contributed new reagents/analytic tools; O.S.I. and H.L. analyzed data; and O.S.I., H.L., and M.B. wrote the paper.

The authors declare no conflict of interest.

This article is a PNAS Direct Submission.

[1]To whom correspondence should be addressed. Email: moritz.buenemann@staff.uni-marburg.de.

This article contains supporting information online at www.pnas.org/lookup/suppl/doi:10.1073/pnas.1715751115/-/DCSupplemental.

Published online April 23, 2018.

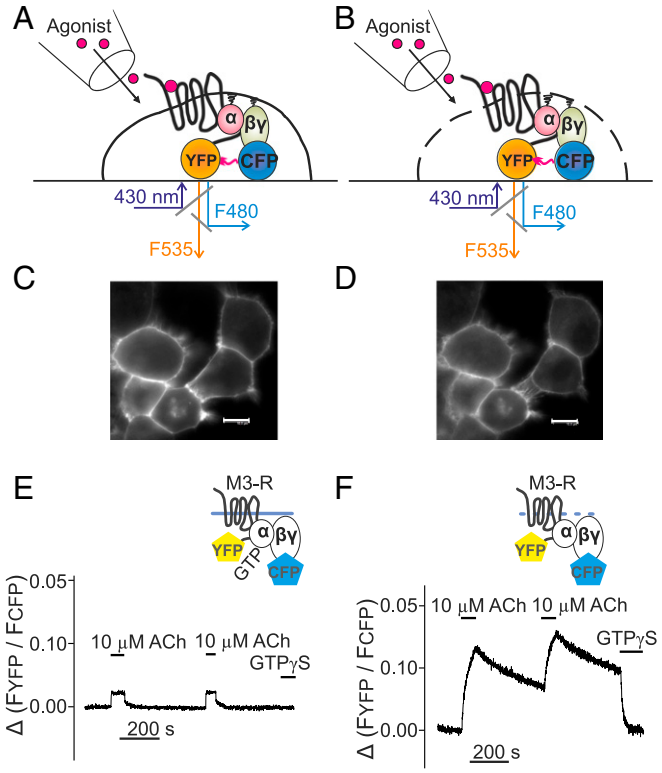

Fig. 1. Assay to measure G-protein–receptor interaction. G_q-protein binding to the M_3–R was measured either in intact (*A*, *C*, and *E*) or permeabilized (*B*, *D*, and *F*) cells by means of brief exposure to saponin as schematically illustrated in *B*. HEK293T cells transfected with M_3–R C-terminally labeled with YFP, $G\alpha_q$-WT, $G\beta_1$-WT, and $G\gamma_2$ N-terminally labeled with CFP (*C*–*F*) were subjected to confocal microscopy and imaged for the CFP fluorescence before (*C*) and after membrane permeabilization (*D*). (Scale bars, 10 μm.) For FRET measurements, cells were excited at 430 nm, and YFP and CFP emission was simultaneously imaged using a dual-emission fluorescence microscope. The YFP/CFP emission ratio derived from a single cell was calculated and plotted over time (*E* and *F*), and the superfusion of cells with agonists or GTPγS occurred as indicated.

dissociation were analyzed by FRET under conditions of GTP depletion. HEK293T cells expressing M_3–R–YFP, $G\alpha_q$, $G\beta_1$ subunits, and CFP-$G\gamma_2$ were subjected to single-cell FRET imaging (Fig. 1*A*), similar to the process described previously (36). In intact non–GTP-depleted cells, we observed a small and rapidly reversible increase in FRET as also shown previously for other receptors (Fig. 1 *C* and *E*) (37). We then permeabilized cells by 2-min exposure to 0.05% saponin (Fig. 1 *B*, *D*, and *F*) to deplete membranes from nucleotides, thus allowing the development of relatively stable agonist–receptor–G-protein complexes. The amplitude of FRET signal in permeabilized cells was substantially higher, indicating a largely increased occupancy of receptors with G proteins (Fig. 1*F*). Most importantly, after withdrawal of agonist, we observed much slower dissociation kinetics of G_q from M_3–R in absence of nucleotides (Fig. 1*E* vs. Fig. 1*F*), which reflects the high intrinsic affinity of G proteins to active receptors under nucleotide-depleted conditions. The rapid drop of the FRET signal in response to GTPγS indicates nucleotide-dependent fast dissociation of the remaining receptor–G-protein complexes (Fig. 1*F*).

Affinity of G Protein to mAChRs Determines GPCR–G-Protein Selectivity. Based on reports that M_3–Rs may also couple to $G_{i/o}$ and even G_s proteins (38), we wanted to quantify the selectivity of M_3–Rs binding to four different classes of G proteins under conditions of nucleotide depletion. Therefore, we compared the agonist [10 μM acetylcholine (ACh)]-evoked FRET signal between fluorescent M_3–R and fluorescent Gβγ subunits when $G\alpha_q$, $G\alpha_o$, $G\alpha_s$, $G\alpha_{13}$, or pcDNA3 instead of Gα was transfected (Fig. 2*A*). As depicted in Fig. 2*A*, there were no significant differences in the small agonist-evoked FRET signal in cells transfected with $G\alpha_s$ or $G\alpha_{13}$ compared with those that were transfected with empty vector instead of cDNA encoding for Gα subunits, indicating no detectable interactions. Although the binding of $G\alpha_s$ and $G\alpha_{13}$ to M_3–R was not detected, these G proteins did bind with high affinity to receptors, such as β-andrenergic receptors (β_1-AR and β_2-AR) and thromboxane TxA_2 receptor (TP-R) (*SI Appendix*, Fig. S1), in accordance with the literature data. Correspondingly, we could not detect G_{13} or G_s activation via stimulation of M_3–R (*SI Appendix*, Fig. S2). However, we observed a robust agonist-induced FRET signal in cells transfected with $G\alpha_o$, which was comparable in amplitude with signals obtained in $G\alpha_q$-expressing cells (Fig. 2*A*, pink vs. black). In experiments studying M_3–R interaction with either G_q or G_o proteins in the presence of high or low concentrations of GDP or GTP, we verified accurate control of nucleotides in permeabilized cells (*SI Appendix*, Fig. S3) and also verified the absence of nucleotide-sensitive preassociation of receptors and G proteins (*SI Appendix*, Fig. S4).

The comparison of G_q and G_o dissociation rates from M_3–R during the withdrawal of agonist in the absence of nucleotides

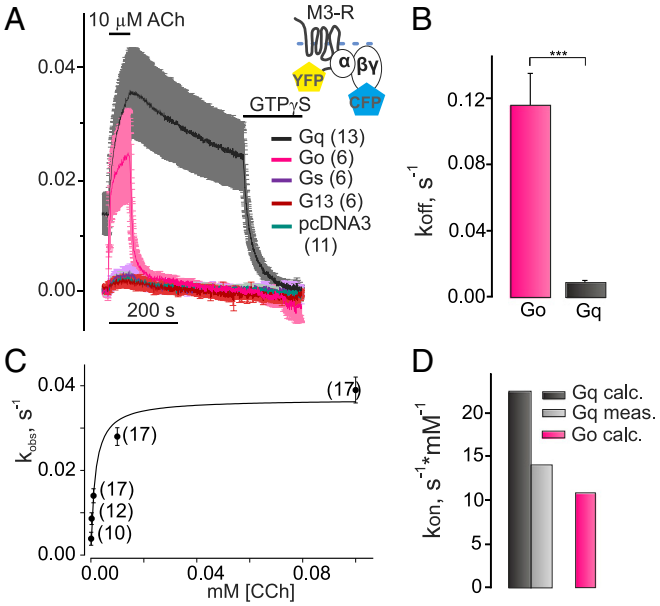

Fig. 2. Selectivity of G protein binding to M_3–R. (*A*) Agonist-dependent association and dissociation of M_3–R with G_o, G_q, G_s, or G_{13} proteins were measured after nucleotide depletion by means of FRET similar to that described in Fig. 1*F*. Average traces of YFP/CFP emission ratio (normalized to initial values) reflecting FRET between YFP-labeled M_3–R and CFP-labeled $G\gamma_2$ subunit are illustrated when $G\alpha_o$-WT (pink curve), $G\alpha_q$-WT (black), G_s (purple), G_{13} (red), or empty pcDNA3 (dark green) was cotransfected. A much faster decay of the FRET signal after withdrawal of agonist was detected for G_o proteins compared with G_q. (*B*) The constants of dissociation (k_{off}; s^{-1}) for G_o and G_q proteins from M_3–R are shown (magenta, $n = 14$; black, $n = 30$, respectively). (*C*) Observed association kinetics (k_{obs}; s^{-1}) of G_q protein with M_3–R under GTP-depleted conditions were plotted over different CCh concentrations and fitted by a hyperbolic function. (*D*) Measured k_{on} value of M_3–R–G_q association kinetics (light gray, G_q meas.) obtained from fitted hyperbolic function using Eq. **2** compared with k_{on}^{C} of G_q (black, G_q calc.) and G_o (magenta, G_o calc.), which were calculated based on steady-state experiments data as shown in Eq. **3**. All data are plotted as means ± SEM for each condition; *n* of each experiment is shown in parentheses if not indicated. Statistical anlysis was performed using one-way ANOVA followed by Student's *t* test (***$P < 0.001$).

PHARMACOLOGY

revealed a significant 13-fold difference (0.009 ± 0.002 and 0.116 ± 0.019 s^{-1}, respectively) (Fig. 2*B* and Fig. 4*A*, exponential fit example), which indicates a lower affinity of the M_3–R–G_o complex. Moreover, since we actually measured interaction of fluorescent Gβγ with fluorescent receptors using overexpressed native Gα subunits for a more accurate comparison between receptor–G-protein coupling, we also performed experiments with fluorescently labeled versions of both $G\alpha_q$ and $G\alpha_o$ as a control. No labeling-associated differences in the dissociation kinetics for both G proteins were detected (*SI Appendix*, Fig. S5). Similarly, long lifetimes of receptor–G-protein complexes were observed for other receptors, such as β_1-, β_2-, and α_{2A}-ARs as well as TP-R, only for G-protein subtypes, which are known to be activated by the respective receptor (*SI Appendix*, Fig. S1). Furthermore, we measured the association kinetics of M_3–R with G_o and G_q proteins under nucleotide-depleted conditions in dependence of the agonist concentration (Fig. 2 *C* and *D*). Based on generally accepted agonist–receptor occupancy models (39, 40), the rates of receptor–G-protein interaction (k_{obs}) should increase with an exponential correlation (Eq. **1**) to the agonist concentration applied. Taking into account that the exponential function is a subcase of a particular hyperbolic sector, k_{on} was calculated as a first derivative of k_{obs} described as hyperbolic function (Eq. **2**):

$$k_{obs} = \frac{P_1 \times x}{P_2 + x}\left(s^{-1}\right) \quad [1]$$

$$k_{on} = (k_{obs})' = \frac{P_1 \times P_2}{(P_2 + x)^2}\left(s^{-1}\cdot mM^{-1}\right) \quad [2]$$

$$k_{on}^{C} = \frac{k_{off}}{EC_{50}}\left(s^{-1}\cdot mM^{-1}\right). \quad [3]$$

Moreover, the k_{on} values for the G_q, G_o, and G_{i2} were also calculated (k_{on}^{C})according to Eq. **3** based on the determined k_{off} values and the apparent EC_{50} values measured under steady-state conditions in permeabilized cells (Eq. **3**, Fig. 3*A*, and *SI Appendix*, Fig. S6). Both k_{on} and k_{on}^{C} values for G_q (Fig. 2*D*) seemed to be relatively similar (22.40 and 14.04 $s^{-1}\cdot mM^{-1}$, respectively). We also attempted to experimentally determine the on-rate for the M_3–R–G_o interaction (*SI Appendix*, Fig. S7); however, in this case, the apparent on-kinetics were faster, and if plotted against the agonist concentration, we failed to fit the data to a simple one-component hyperbolic function (*SI Appendix*, Table S1). Obviously, the measured and calculated association kinetics did not reflect the differences in coupling preference for G_q over G_o proteins. This suggests—at least for the M_3–R—that the lifetimes of the ternary complexes play a major role in the determination of receptor–G-protein selectivity.

The Difference in G_o and G_q Affinity to M_3–R Reflects Coupling Efficiency. To experimentally verify whether the measured k_{on} and k_{off} were realistic, we next determined steady-state binding curves for the carbachol (CCh)-induced nucleotide-free complex formation of M_3–R with $G\alpha_q$- or $G\alpha_o$-containing G proteins in dependence of agonist concentration by determining the stable plateau reached after agonist application (Fig. 3 *A*, black vs. pink and *B*). The concentration–response curve of G_o binding to M_3–R was found to be 16.5-fold (right shifted in comparison with G_q; EC_{50} = 10.68 ± 0.32 and 0.64 ± 0.04 μM, respectively), which indicates a higher affinity of binding of G_q to M_3–R compared with G_o. Under these conditions, we determined the G-protein/receptor expression ratio to be two- to sixfold (*SI Appendix*, Fig. S8) and also detected no major alterations of Gβγ expression in dependence of the coexpressed Gα subtype (*SI Appendix*, Fig. S9).

To test whether the stability of the ternary complex correlates with the efficiency of G-protein activation, we determined G_o- and G_q-protein coupling efficiency to M_3–R (Fig. 3 *C* and *D*) by measuring FRET between YFP-labeled Gα and CFP-labeled Gβγ subunits (41) in thousands of nonpermeabilized adherent transiently transfected cells (Fig. 3*D*) in a 96-well format. Similar to the binding data, the concentration–response curve of $G\alpha_o$ activation (EC_{50} = 0.79 ± 0.01 μM) by M_3–R was 6.6-fold right shifted in comparison with $G\alpha_q$ activation (EC_{50} = 0.12 ± 0.01 μM) (Fig. 3*C*, pink vs. black). Considering our findings regarding the on-kinetics of G_o and G_q binding to activated M_3–R, this

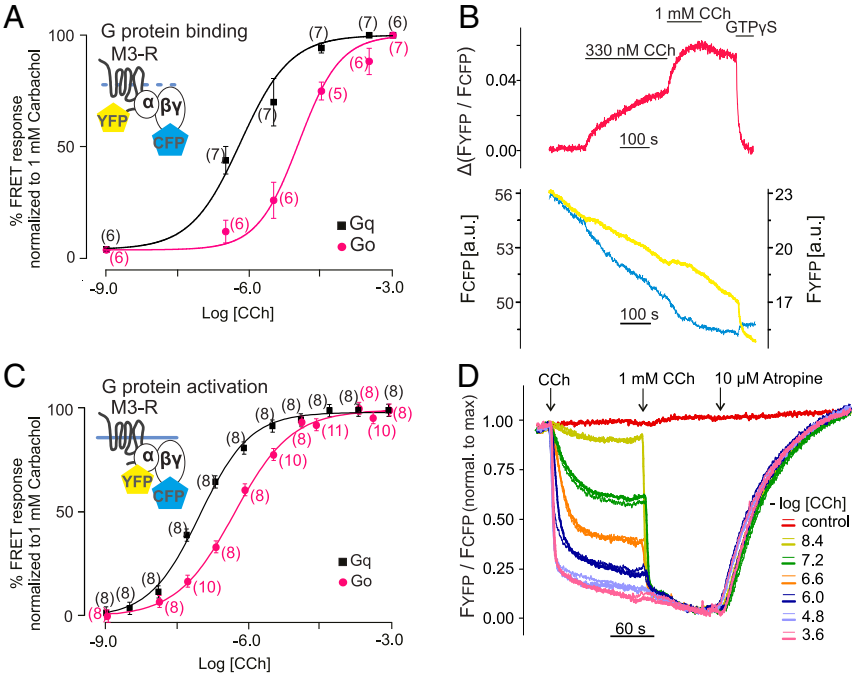

Fig. 3. Comparison of receptor–G-protein binding and activation of G proteins. (*A*) Concentration–response curves of G_q (black) and G_o (pink) binding to M_3–R under GTP-free conditions. FRET imaging in single permeabilized cells was performed as described in Fig. 1*F*. Increasing concentrations of CCh were applied as shown in a representative trace of a G_q-expressing cell (*B*). The change of YFP/CFP emission ratio was normalized to the amplitude observed on application of saturating CCh concentration (1 mM; maximum response) and the YFP/CFP ratio measured under the application of GTPγS (minimum response). To achieve steady-state conditions at low CCh concentrations (under 100 nM), cells were incubated for 10 min. (*C* and *D*) Concentration–response curves of G_q and G_o activation by M_3–R were determined in intact cells using established G-protein FRET assays (61). (*D*) Representative traces of FRET between YFP-labeled Gα subunit and CFP-labeled $G\gamma_2$ subunit were measured in duplicates (overflow technique) simultaneously in 12 individual wells derived from a 96-well plate and normalized to the maximal response (1 mM CCh). All concentration–response data are represented as means ± SEM for each condition; *n* of each experiment is shown in parentheses. Statistical analysis was performed by one-way ANOVA with Bonferroni post hoc test ($P < 0.05$).

result shows that the affinity of the mAChRs–G-protein interaction underlying G-protein selectivity is primarily reflected by the stability (lifetime) of the complex and correlates closely with the coupling efficiency. Moreover, we measured dissociation kinetics of M_3–R–$G_{i/o}$ proteins complexes in dependence of $G\alpha_i$ subtypes and found no significant differences for $G\alpha_{i1}$, $G\alpha_{i2}$, and $G\alpha_{i3}$ (Fig. 4*D* and *SI Appendix*, Fig. S10*A*). Similar results were obtained for M_1–R (Fig. 4 *A* and *B* and *SI Appendix*, Fig. S10 *B* and *E*).

To test for the $G_{i/o}$-subtype selectivity of M_2–R, we repeated similar experiments for M_2–R. Here, we observed a higher amplitude and slightly enhanced complex stability for $G\alpha_o$ and $G\alpha_{i2}$ compared with $G\alpha_{i1}$ and $G\alpha_{i3}$, as the calculated k_{off} values of $G\alpha_o$ and $G\alpha_{i2}$ from M_2–R were twofold smaller in comparison with $G\alpha_{i1}$ and $G\alpha_{i3}$, a result that correlates with the G-protein homology within the G_i family (Fig. 4*C* and *SI Appendix*, Fig. S10 *D* and *F*). Also, as expected, no binding of $G\alpha_q$ to M_2–R in the absence of nucleotides was detected (*SI Appendix*, Fig. S10*C*). A summary of all k_{off} values is shown in *SI Appendix*, Table S2.

Agonist Affinity Is Not Crucial for G_q- and G_o-Protein Affinity to M_3–R. To activate mAChRs, we used three different agonists exhibiting different affinities and efficacies toward binding and activation: ACh, its synthetic analog CCh, and the partial agonist arecoline (Are) (42). Thus, we also addressed the question of whether the type of the ligand can affect the affinity of the G protein to the receptor. HEK293T cells were transiently transfected and permeabilized as mentioned above. Single cells were first stimulated with ACh and after its withdrawal, stimulated a second time with CCh or Are (*SI Appendix*, Fig. S11*A*). This procedure allows a comparison of the dissociation kinetics of G-protein–receptor complexes in the same cell, meaning equal expression levels of interacting proteins. We observed similar dissociation rates of G_q from ACh-, CCh-, and Are-activated M_3–R (*SI Appendix*, Fig. S11 *A* and *B*). Relatedly, the dissociation kinetics of G_o from M_3–R were not significantly different for all three agonists (*SI Appendix*, Fig. S11 *C* and *D*). Thus, we could conclude that, at least in the case of agonists with moderate to low affinity, the stability of the G-protein–receptor complex is an intrinsic property of the mAChR–G-protein pair and not influenced by the agonist affinity.

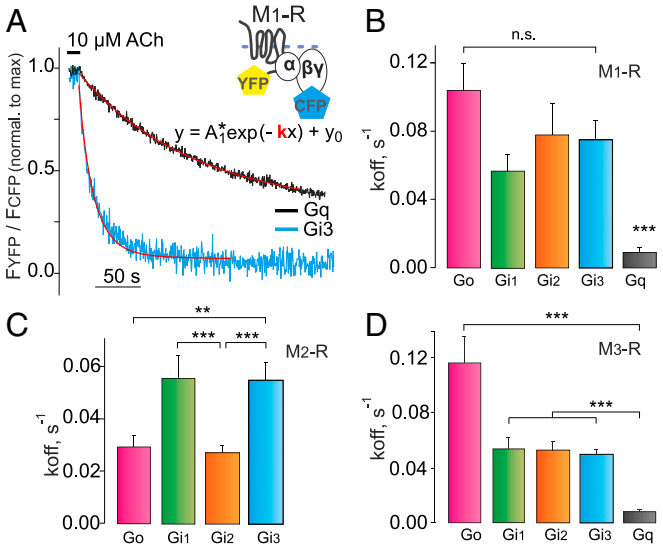

Fig. 4. Comparison of the stability of G-protein–receptor complexes. Decay kinetics of receptor–G-protein complexes were determined in response to agonist withdrawal for M_1–, M_2–, and M_3–Rs and different members of the $G_{i/o}$- and G_q-protein family in experiments similar to those shown in Fig. 1*F*. (*A*) Examples of exponential curve fittings to the decline in the YFP/CFP ratio after agonist withdrawal for M_1–R and G_{i3} (blue) or G_q (black) protein. The constants of dissociation (k_{off}; s^{-1}) of G_{i1}, G_{i2}, G_{i3}, G_o, and G_q proteins (green, orange, blue, magenta, and black, respectively, in all bar graphs) were calculated for M_1– (*B*), M_2– (*C*), and M_3–Rs (*D*). Calculated k_{off} (s^{-1}) values, including the replication numbers (*n*), are given in *SI Appendix*, Table S2. The data are represented as means ± SEM. (Data for G_o and G_q are taken from Fig. 2*B* for comparison.) Normalization of alterations in FRET was performed as described in Fig. 2. Statistical analysis was performed using one-way ANOVA followed by Dunnett's multiple comparison test (**$P < 0.01$; ***$P < 0.001$; n.s., $P \geq 0.05$).

Discussion

Understanding the molecular mechanism of selectivity and efficiency of receptor-mediated G-protein activation is one of the key research topics in the field of GPCR physiology and pharmacology. Based on the fact that agonist–receptor–G-protein complexes exhibit the highest stability in absence of nucleotides (43, 44), we quantified the affinity of different G proteins to M_1–, M_2–, and M_3–Rs (22, 28, 45) by means of FRET imaging on permeabilized membranes of single cells. By laminar superfusion of these membranes, we ensured excellent control of agonist and nucleotides (*SI Appendix*, Fig. S3) and resolved the dynamics of interactions between nucleotide-free G proteins with several different receptors. The lifetime of receptor–G-protein complexes was determined by measuring complex dissociation in response to withdrawal of agonist and was longest for those complexes that contained G-protein subtypes that are known to be activated best by the respective receptor (Figs. 2 and 4 and *SI Appendix*, Figs. S1 and S10). Our detailed analysis (Fig. 2*B* vs. Fig. 2 *C* and *D* and *SI Appendix*, Fig. S7) of M_3–R revealed that the lifetime of the nucleotide-free GPCR–G-protein complex (rather than the association kinetics) is the major determinant for the differences in affinity of these complexes (Fig. 3*A* and *SI Appendix*, Fig. S6).

Unlike the dissociation kinetics of the nucleotide-free receptor–G-protein complex, the steady-state and on-rate measurements might not exclusively be restricted to complexes after GDP release but also include initially GDP-bound G proteins, although these do not contribute a lot to the overall signal (*SI Appendix*, Fig. S3 *B* and *D*). GDP release is much faster for G_o (46) than for G_q (47), which needs to be considered. We attempted to calculate the k_{on} of GPCR–G-protein interactions in native cell membranes. The correlation of apparent M_3–R–G_q association kinetics and agonist concentration is consistent with a hyperbolic function (Fig. 2*C*), allowing us to determine the k_{on} directly. The resulting value of $k_{on} = 22.4\ s^{-1}{\cdot}mM^{-1}$ was remarkably close to the $k_{on} = 14.1\ s^{-1}{\cdot}mM^{-1}$ calculated by division of k_{off} (Fig. 2 *A* and *B*) by the EC_{50} value (Fig. 3*A* and *SI Appendix*, Table S1), clearly indicating the applicability of our method. Based on the much faster equilibration kinetics of agonist binding to non-G-protein–bound muscarinic receptors (48), the kinetics of agonist-induced receptor–G-protein complex formation under nucleotide-free conditions is probably a close approximation to the optimal situation of G proteins binding to equilibrated agonist–receptor complexes. In the case of M_3–R–G_o interaction, the correlation of apparent association kinetics of G_o proteins and M_3–R with the agonist concentration is best explained by a two-component hyperbolic function (*SI Appendix*, Fig. S7). A comparison of the correspondingly determined on-rates with k_{on} (calculated using Eq. **3**) revealed, even with the slower on-rate, a fivefold deviation from the calculated k_{on}. Possible reasons for this could be effects due to the above-mentioned multistep binding reaction. This might affect the apparent association kinetics of receptors and G proteins and complicates interpretation of the measured k_{on}. Therefore, at the current research stage, we propose that measuring the off-rates of the complex together with steady-state association gives a more robust quantitative correlate of the affinity of the subtype-specific receptor–G-protein complex.

PHARMACOLOGY

Our results show that both the steady-state curves of G protein binding to the M_3–Rs as well as the dissociation kinetics of this complex quantitatively reflect M_3–R–G-protein selectivity (Fig. 3). Specifically, the dissociation kinetics of G_o protein from M_3– and M_1–Rs were 13-fold faster in comparison with G_q (Figs. 2 *A* and *B* and 4 *B* and *D* and *SI Appendix*, Fig. S10 *A*, *B*, and *E*). Similarly, we observed an approximate 16.5-fold right shift of the concentration–response curves of G_o proteins binding to M_3–R in comparison with G_q (Fig. 3*A*). A quantitatively similar 6.6-fold difference in coupling efficiency of G_o and G_q to M_3–R, measured in an FRET-based G-protein activation assay in intact cells (Fig. 3*C*), suggests that the efficacy of coupling to a certain G-protein subtype is indeed reflected in the relative M_3–R–G-protein affinity and can thus be detected by measurement of the lifetime of the G-protein–receptor complex. For moderate- to low-affinity agonists with different efficacy, we could so far not detect differences in the stability of M_3–R–G_q or G_o complexes. An important finding was that the G_q-coupled and evolutionary close M_1– and M_3–Rs exhibited very close ternary complex stabilities, with a very similar pattern for the different G-protein subtypes (Fig. 4 *A*, *B*, and *D* and *SI Appendix*, Fig. S10 *A*, *B*, and *E*). Remarkably, the stability of the complex of different GPCRs under investigation with their best coupling G protein varied over at least two orders of magnitude, being lowest for M_2–R–G_o protein complexes (lifetime only a few seconds) (*SI Appendix*, Table S2) and highest for TP-R–G_{13} and β-AR–Gs complexes (lifetime >200 s) (*SI Appendix*, Fig. S1 *A*, *C*, and *E*), which likely reflect the parallel evolution of the coupling mechanism (49). In light of the recent advances in understanding the allosteric effect of G protein binding (or mimicking nanobodies) to the M_2–R–agonist interaction, specifically the closure of a tyrosine lid on the extracellular side of the agonist exit path (13, 50, 51), our results that M_2–R–G_o interaction is very short lived may be somewhat unexpected. However, they are not contradictory to published results, as the lifetime of M_2–R–G_o complexes was not addressed in previous studies. The reliability of the method that we developed was also confirmed by testing other G-protein classes. For instance, we were unable to detect G_s or G_{13} binding to M_3–R or M_1–R under nucleotide-depleted conditions (Fig. 2*A* and *SI Appendix*, Fig. S10*B*) or to observe activation of these G proteins measured by means of FRET (*SI Appendix*, Fig. S2).

Furthermore, we screened other G_i family proteins, and although we could not observe significant differences in the affinities of G_i proteins to M_3– or M_1–Rs, M_2–R did show a higher specificity for G_o and G_{i2} over G_{i1} and G_{i3} (Fig. 4*C* and *SI Appendix*, Fig. S10 *D* and *F*). This distinct affinity profile of GPCR is also supported by recently delineated GPCR "fingerprints" determined as the efficiency of G-protein activation by different GPCRs (52). Moreover, recent computational and evolutionary studies assume that the selectivity mechanism of GPCRs is likely disclosed on the G-protein level (15, 49). Thus, we conclude that receptor–G-protein affinity represents a major determinant for receptor–G-protein subtype selectivity. We could essentially attribute the observed differences in the affinity of G_o versus G_q toward active M_3–Rs to differences in the lifetime of the complex, suggesting that the apparent on-rate of complex formation is less important for defining coupling selectivity.

The potential and distinctive advantage of our FRET-based nucleotide-free method over biochemical assays is the ability to perform experiments in a regular membrane environment. By excluding the steps of protein purification and protein reconstitution (53, 54), a remarkably high degree of signal specificity is still exhibited. This is particularly important, as G proteins are well-known to be very sensitive to detergents (55). Furthermore, this method is easily accessible to all GPCRs and G proteins and can be used as a reliable way to quantify GPCR–G-protein specificity.

Materials and Methods

Chemicals. DMEM, FCS, PBS, penicillin/streptomycin, L-glutamine, and trypsin-EDTA were from Biochrom. Saponin was purchased from AppliChem. All other substances were purchased from Sigma-Aldrich.

Plasmids. cDNAs for $G\alpha_q$; $G\alpha_q$-YFP (56); $G\beta_1$-WT; $G\gamma_2$-WT; $G\alpha_o$-YFP (C351I) (57); $G\alpha_{i1}$ (C351I)-, $G\alpha_{i2}$-, $G\alpha_{i3}$- (58), and $G\alpha_o$-WT (59); CFP-$G\gamma_2$ (37); and M_3–R–YFP (48) were described previously. The M_3–R was obtained from the Missouri S&T cDNA Resource Center. M_3–R–mTurquoise fluorescent protein was cloned analogously to M_3–R–YFP.

Cell Culture and Transfection. All experiments were carried out in HEK293T cells (a gift from Dr. Martin Lohse, Institute of Pharmacology, Würzburg, Germany). Cells were cultured in high-glucose DMEM supplemented with 10% FBS, 2 mM L-glutamine, 100 U/mL penicillin, and 0.1 mg/mL streptomycin at 37 °C and 5% CO_2. Cells were transiently transfected with 0.5 μg DNA (6-cm dish) of each particular mAChR-YFP, 1.5 μg DNA Gα-WT of interest (if not otherwise indicated), 0.5 $G\beta_1$-WT, 0.2 CFP-$G\gamma_2$, and 0.3 pcDNA3 (if not otherwise indicated) using Effectene Transfection Reagent according to the manufacturer's instructions (Qiagen). For the G-protein activation, HEK293T cells were transfected with (micrograms DNA, 6-cm dish) 0.5 μg M_3–R–WT, 0.8 μg Gα-YFP of interest, 0.5 μg $G\beta_1$-WT, and 0.2 μg CFP-$G\gamma_2$. Experiments were performed 48 h after transfection at room temperature on cells, which were plated into six-well plates with 25-mm coverslips (cover glasses were preincubated 30 min with poly-L-lysine) 1 d after transfection.

Permeabilization Procedure. Coverslips with transiently transfected HEK293T cells were fixed in a microscope chamber and washed once with external buffer (137 mM NaCl, 5.4 mM KCl, 10 mM Hepes, 2 mM $CaCl_2$, 1 mM $MgCl_2$, pH 7.3). To permeabilize cells, coverslips were incubated for 2 min with 0.05% saponin and afterward washed five times with internal buffer (100 mM K^+-aspartate, 30 mM KCl, 10 mM Hepes, 5 mM EGTA, 1 mM $MgCl_2$, 10 mM NaCl, pH 7.35.), inducing the depletion of GTP and GDP (60).

Single-Cell FRET Imaging. The FRET measurements were performed on single cells selected for membrane staining of YFP and CFP fluorescence. The round shape of cells was taken as an indicator of proper permeabilization. Dual-emission imaging of YFP and CFP of a single cell (or its membrane) was performed as previously described in the work by Milde et al. (36) and modified as described in *SI Appendix, SI Methods*. Individual traces are shown as either absolute or relative YFP/CFP emission ratio changes. Absolute changes in YFP/CFP emission ratio were calculated as the differences in average values of the last 10 s before or after an event. The relative change of F_{YFP}/F_{CFP} was calculated by normalization to the maximum peak after application of saturating agonist concentration relative to the G-protein–state determined by application of GTPγS. As a measure of the affinity of the G-protein–receptor complex, dissociation kinetics of the complex were measured under nucleotide-free conditions in response to agonist withdrawal. Resulting data of the offset kinetics (decrease in FRET) were fitted by a monoexponential function.

Multiple-Cell FRET Imaging. The efficiency of G-protein activation by the receptor of interest was determined by means of a multiple-cell FRET assay in intact cells transiently transfected as previously described in the work by Frank et al. (59). Transfected HEK293T cells cultivated in 12-well strips (TC; 96-well format; Greiner Bio-One) were washed with and maintained in external buffer A (137 mM NaCl, 5.4 mM KCl, 1.0 mM $MgCl_2$, 2.0 mM $CaCl_2$, 10 mM Hepes, 2% Brilliant Black) at 32.5 °C. The final volume was 275 μL per well. Injections of test compounds (agonists and antagonists) were made with a volume of 22 μL added gradually with gentle up and down movements of the 12-channel injecting unit equipped with 50-mm needles (1.2-mm diameter), resulting in a 13.5-fold dilution of stock solutions. Alternatively, cells were stimulated with an overflow apparatus, allowing almost immediate (<3 s) change of the standard buffer to induce receptor stimulation (Fig. 3*D*). Details for the optical equipment are given in *SI Appendix, SI Methods*.

Data Processing. Fluorescence intensities were acquired using the imaging software NIS-Elements advanced research (Nikon Corporation). Values are given as means ± SEM of *n* experiments. Other programs used for the analysis are given in *SI Appendix, SI Methods*.

ACKNOWLEDGMENTS. We thank Prof. Dr. Cornelius Krasel for the fruitful discussions and helpful comments. This work was partially funded by the Deutscher Academischer Austauschdienst.

1. Simon MI, Strathmann MP, Gautam N (1991) Diversity of G proteins in signal transduction. *Science* 252:802–808.
2. Hillenbrand M, Schori C, Schöppe J, Plückthun A (2015) Comprehensive analysis of heterotrimeric G-protein complex diversity and their interactions with GPCRs in solution. *Proc Natl Acad Sci USA* 112:E1181–E1190.
3. Schultz G, Rosenthal W, Hescheler J, Trautwein W (1990) Role of G proteins in calcium channel modulation. *Annu Rev Physiol* 52:275–292.
4. Siderovski DP, Willard FS (2005) The GAPs, GEFs, and GDIs of heterotrimeric G-protein alpha subunits. *Int J Biol Sci* 1:51–66.
5. Patel M, et al. (2014) Gα13/PDZ-RhoGEF/RhoA signaling is essential for gastrin-releasing peptide receptor-mediated colon cancer cell migration. *Mol Pharmacol* 86: 252–262.
6. Allgeier A, et al. (1994) The human thyrotropin receptor activates G-proteins Gs and Gq/11. *J Biol Chem* 269:13733–13735.
7. Xiao R-P, Ji X, Lakatta EG (1995) Functional coupling of the β 2-adrenoceptor to a pertussis toxin-sensitive G protein in cardiac myocytes. *Mol Pharmacol* 47:322–329.
8. Eason MG, Kurose H, Holt BD, Raymond JR, Liggett SB (1992) Simultaneous coupling of α 2-adrenergic receptors to two G-proteins with opposing effects. Subtype-selective coupling of α 2C10, α 2C4, and α 2C2 adrenergic receptors to Gi and Gs. *J Biol Chem* 267:15795–15801.
9. Kilts JD, et al. (2000) β(2)-adrenergic and several other G protein-coupled receptors in human atrial membranes activate both G(s) and G(i). *Circ Res* 87:705–709.
10. Hermans E (2003) Biochemical and pharmacological control of the multiplicity of coupling at G-protein-coupled receptors. *Pharmacol Ther* 99:25–44.
11. Herrlich A, et al. (1996) Involvement of Gs and Gi proteins in dual coupling of the luteinizing hormone receptor to adenylyl cyclase and phospholipase C. *J Biol Chem* 271:16764–16772.
12. Thal DM, et al. (2016) Crystal structures of the M1 and M4 muscarinic acetylcholine receptors. *Nature* 531:335–340.
13. Haga K, et al. (2012) Structure of the human M2 muscarinic acetylcholine receptor bound to an antagonist. *Nature* 482:547–551.
14. Li Z, Zhou X, Dai Z, Zou X (2012) Classification of G proteins and prediction of GPCRs-G proteins coupling specificity using continuous wavelet transform and information theory. *Amino Acids* 43:793–804.
15. Flock T, et al. (2015) Universal allosteric mechanism for Gα activation by GPCRs. *Nature* 524:173–179.
16. Gudermann T, Kalkbrenner F, Schultz G (1996) Diversity and selectivity of receptor-G protein interaction. *Annu Rev Pharmacol Toxicol* 36:429–459.
17. Dippel E, Kalkbrenner F, Wittig B, Schultz G (1996) A heterotrimeric G protein complex couples the muscarinic m1 receptor to phospholipase C-β. *Proc Natl Acad Sci USA* 93:1391–1396.
18. Berstein G, et al. (1992) Reconstitution of agonist-stimulated phosphatidylinositol 4,5-bisphosphate hydrolysis using purified m1 muscarinic receptor, Gq/11, and phospholipase C-β 1. *J Biol Chem* 267:8081–8088.
19. Leach K, Simms J, Sexton PM, Christopoulos A (2012) Structure-function studies of muscarinic acetylcholine receptors. *Handb Exp Pharmacol* 208:29–48.
20. Smrcka AV, Hepler JR, Brown KO, Sternweis PC (1991) Regulation of polyphosphoinositide-specific phospholipase C activity by purified Gq. *Science* 251: 804–807.
21. Zhang Y, et al. (2011) Activation of M3 muscarinic receptors inhibits T-type Ca(2+) channel currents via pertussis toxin-sensitive novel protein kinase C pathway in small dorsal root ganglion neurons. *Cell Signal* 23:1057–1067.
22. Burford NT, Tobin AB, Nahorski SR (1995) Differential coupling of m1, m2 and m3 muscarinic receptor subtypes to inositol 1,4,5-trisphosphate and adenosine 3′,5′-cyclic monophosphate accumulation in Chinese hamster ovary cells. *J Pharmacol Exp Ther* 274:134–142.
23. Wess J (1993) Molecular basis of muscarinic acetylcholine receptor function. *Trends Pharmacol Sci* 14:308–313.
24. Burford NT, Nahorski SR (1996) Muscarinic m1 receptor-stimulated adenylate cyclase activity in Chinese hamster ovary cells is mediated by Gs α and is not a consequence of phosphoinositidase C activation. *Biochem J* 315:883–888.
25. Ramachandran J, et al. (1989) Structural and functional diversity of muscarinic acetylcholine receptor subtypes. *Prog Clin Biol Res* 289:327–339.
26. Dell'Acqua ML, Carroll RC, Peralta EG (1993) Transfected m2 muscarinic acetylcholine receptors couple to G α i2 and G α i3 in Chinese hamster ovary cells. Activation and desensitization of the phospholipase C signaling pathway. *J Biol Chem* 268: 5676–5685.
27. Albert PR, Robillard L (2002) G protein specificity: Traffic direction required. *Cell Signal* 14:407–418.
28. Wess J (1998) Molecular basis of receptor/G-protein-coupling selectivity. *Pharmacol Ther* 80:231–264.
29. Wong SK-F (2003) G protein selectivity is regulated by multiple intracellular regions of GPCRs. *Neurosignals* 12:1–12.
30. Dohlman HG, Thorner J, Caron MG, Lefkowitz RJ (1991) Model systems for the study of seven-transmembrane-segment receptors. *Annu Rev Biochem* 60:653–688.
31. De Lean A, Stadel JM, Lefkowitz RJ (1980) A ternary complex model explains the agonist-specific binding properties of the adenylate cyclase-coupled β-adrenergic receptor. *J Biol Chem* 255:7108–7117.
32. Oldham WM, Hamm HE (2008) Heterotrimeric G protein activation by G-protein-coupled receptors. *Nat Rev Mol Cell Biol* 9:60–71.
33. Cerione RA, et al. (1984) The mammalian β 2-adrenergic receptor: Reconstitution of functional interactions between pure receptor and pure stimulatory nucleotide binding protein of the adenylate cyclase system. *Biochemistry* 23:4519–4525.
34. Cerione RA, et al. (1985) Specificity of the functional interactions of the β-adrenergic receptor and rhodopsin with guanine nucleotide regulatory proteins reconstituted in phospholipid vesicles. *J Biol Chem* 260:1493–1500.
35. Rubenstein RC, Linder ME, Ross EM (1991) Selectivity of the β-adrenergic receptor among Gs, Gi's, and Go: Assay using recombinant alpha subunits in reconstituted phospholipid vesicles. *Biochemistry* 30:10769–10777.
36. Milde M, Rinne A, Wunder F, Engelhardt S, Bünemann M (2013) Dynamics of Gαi1 interaction with type 5 adenylate cyclase reveal the molecular basis for high sensitivity of Gi-mediated inhibition of cAMP production. *Biochem J* 454:515–523.
37. Hein P, Bünemann M (2009) Coupling mode of receptors and G proteins. *Naunyn Schmiedebergs Arch Pharmacol* 379:435–443.
38. Jones SV, Heilman CJ, Brann MR (1991) Functional responses of cloned muscarinic receptors expressed in CHO-K1 cells. *Mol Pharmacol* 40:242–247.
39. Kenakin T (2008) Receptor theory. *Curr Protoc Pharmacol* 1:1.2.
40. Pierre N (2011) Determination of association (kon) and dissociation (koff) rates of spiperone on the dopamine D2 receptor using a platform for GPCR applications. *Am Lab* 2013:2–4.
41. Vilardaga J-P, Bünemann M, Krasel C, Castro M, Lohse MJ (2003) Measurement of the millisecond activation switch of G protein-coupled receptors in living cells. *Nat Biotechnol* 21:807–812.
42. Stamatiou R, et al. (2014) Long-term exposure to muscarinic agonists decreases expression of contractile proteins and responsiveness of rabbit tracheal smooth muscle cells. *BMC Pulm Med* 14:39.
43. Christopoulos A, Kenakin T (2002) G protein-coupled receptor allosterism and complexing. *Pharmacol Rev* 54:323–374.
44. Roberts DJ, Waelbroeck M (2004) G protein activation by G protein coupled receptors: Ternary complex formation or catalyzed reaction? *Biochem Pharmacol* 68:799–806.
45. Kostenis E, Zeng FY, Wess J (1998) Structure-function analysis of muscarinic acetylcholine receptors. *J Physiol Paris* 92:265–268.
46. Higashijima T, Ferguson KM, Sternweis PC, Smigel MD, Gilman AG (1987) Effects of Mg2+ and the β γ-subunit complex on the interactions of guanine nucleotides with G proteins. *J Biol Chem* 262:762–766.
47. Mukhopadhyay S, Ross EM (1999) Rapid GTP binding and hydrolysis by G(q) promoted by receptor and GTPase-activating proteins. *Proc Natl Acad Sci USA* 96:9539–9544.
48. Hoffmann C, et al. (2012) Comparison of the activation kinetics of the M3 acetylcholine receptor and a constitutively active mutant receptor in living cells. *Mol Pharmacol* 82:236–245.
49. Flock T, et al. (2017) Selectivity determinants of GPCR-G-protein binding. *Nature* 545: 317–322.
50. Kruse AC, et al. (2013) Activation and allosteric modulation of a muscarinic acetylcholine receptor. *Nature* 504:101–106.
51. DeVree BT, et al. (2016) Allosteric coupling from G protein to the agonist-binding pocket in GPCRs. *Nature* 535:182–186.
52. Carr R, 3rd, et al. (2016) Interdicting Gq activation in airway disease by receptor-dependent and receptor-independent mechanisms. *Mol Pharmacol* 89:94–104.
53. Lee E, Linder ME, Gilman AG (1994) Expression of G-protein α subunits in Escherichia coli. *Methods Enzymol* 237:146–164.
54. Linder ME, Ewald DA, Miller RJ, Gilman AG (1990) Purification and characterization of Go α and three types of Gi α after expression in Escherichia coli. *J Biol Chem* 265: 8243–8251.
55. Sýkora J, Bouřová L, Hof M, Svoboda P (2009) The effect of detergents on trimeric G-protein activity in isolated plasma membranes from rat brain cortex: Correlation with studies of DPH and Laurdan fluorescence. *Biochim Biophys Acta* 1788:324–332.
56. Hughes TE, Zhang H, Logothetis DE, Berlot CH (2001) Visualization of a functional Gαq-green fluorescent protein fusion in living cells. *J Biol Chem* 276:4227–4235.
57. Bünemann M, Frank M, Lohse MJ (2003) Gi protein activation in intact cells involves subunit rearrangement rather than dissociation. *Proc Natl Acad Sci USA* 100: 16077–16082.
58. Wise A, Watson-Koken M-A, Rees S, Lee M, Milligan G (1997) Interactions of the α2A-adrenoceptor with multiple Gi-family g-proteins: Studies with pertussis toxin-resistant g-protein mutants. *Biochem J* 321:721–728.
59. Frank M, Thümer L, Lohse MJ, Bünemann M (2005) G Protein activation without subunit dissociation depends on a Gα(i)-specific region. *J Biol Chem* 280:24584–24590.
60. Hommers LG, Klenk C, Dees C, Bünemann M (2010) G proteins in reverse mode: Receptor-mediated GTP release inhibits G protein and effector function. *J Biol Chem* 285:8227–8233.
61. Wolters V, Krasel C, Brockmann J, Bünemann M (2015) Influence of Gαq on the dynamics of m3-acetylcholine receptor-G-protein-coupled receptor kinase 2 interaction. *Mol Pharmacol* 87:9–17.